Journal of Materials Chemistry

Cite this: *J. Mater. Chem.*, 2012, **22**, 3471

www.rsc.org/materials

PAPER

Reduced graphene oxide/nickel nanocomposites: facile synthesis, magnetic and catalytic properties†

Zhenyuan Ji,[ab] Xiaoping Shen,*[a] Guoxing Zhu,[a] Hu Zhou[c] and Aihua Yuan[c]

Received 20th September 2011, Accepted 25th November 2011
DOI: 10.1039/c2jm14680k

Graphene, which possesses unique nanostructure and excellent properties, is considered a low cost alternative to carbon nanotubes in nanocomposites. In this paper, we demonstrate a facile *in situ* reduction approach for the synthesis of reduced graphene oxide/Ni (RGO/Ni) nanocomposites with different morphologies. The concentration of nickel ions has a great influence on the morphology of the RGO/Ni nanocomposites and an interesting RGO-wrapped nanostructure was obtained. Magnetic studies reveal a room-temperature ferromagnetic behavior of the RGO/Ni nanocomposites. The catalytic activities of the RGO/Ni nanocomposites were investigated for the reduction of *p*-nitrophenol by $NaBH_4$. It was found that the nanocomposites show higher catalytic activity compared with the unsupported Ni nanoparticles. The catalytic performance of the RGO/Ni nanocomposites was even better than the RANEY® Ni catalyst. Moreover, after completion of the reaction the nanocomposite catalyst can be easily re-collected from the reaction system by a magnet. Thus, the RGO/Ni nanocomposites obtained in this work may find applications in catalysis, data storage, targeted drug transportation and magnetic resonance imaging technologies.

Introduction

Graphene, which is a single or few layer sheet of graphitic carbon, offers great advantages owing to its high surface area, good conductivity and excellent mechanical properties,[1] and has become a "rising star" in the field of material science. It has motivated the development of new composite materials for nanoelectronics, supercapacitors, batteries, photovoltaics, catalysts, and related devices.[2–8] Up to now, numerous methods have been developed for the production of graphene sheets including micromechanical exfoliation, thermal expansion of graphite,[9–11] chemical vapor deposition[1,12] and solution-based chemical reduction of exfoliated graphite oxide to RGO.[13–16] Among these methods, chemical reduction of exfoliated graphite oxide is the most suitable approach for the efficient production of processable graphene sheets owing to its low-cost and massive scalability.[15] Graphite oxide can be readily dispersed in water to yield stable dispersions by simple sonication on account of the presence of oxygen-containing functional groups such as hydroxyl, epoxide and carboxyl moieties.[17] Furthermore, these oxygen functional groups can act as nucleation centers or anchoring sites for the landing of nanoparticles,[18] limiting the nanoparticles growth, improving the stability and dispersion of nanoparticles on RGO. At the same time, these nanoparticles can help to enlarge the interplanar spacing of the RGO especially when they are in solid state, avoid them aggregating into graphitic structure, and maintain the excellent properties of individual RGO nanosheets. Moreover, recent studies have shown that the synergistic coupling between nanomaterials and RGO can lead to enhanced performance or even a new property that are not found in the individual components.[19–22]

Magnetic nanoparticles are of great interest for researchers from a wide range of disciplines, including magnetic fluids,[23] data storage,[24] biotechnology/biomedicine,[25] catalysis,[26,27] magnetic resonance imaging,[28,29] *etc.* Nowadays, it is well realized that the dispersion of magnetic nanoparticles on RGO sheets potentially provides a new way to develop novel catalytic, magnetic, adsorbing, and electrode materials.[30–33] With this in mind, RGO-based nanocomposites containing magnetic nanoparticles (Fe_3O_4, $ZnFe_2O_4$, $CoFe_2O_4$, Co) have recently been reported.[33,34–39] Ni nanoparticles are important magnetic materials and have found applications as catalysts for hydrogenation of nitrobenzene[40] and thermal decomposition of ammonium perchlorate,[41] as well as fillers for magnetic inks[42] or ferrofluids,[43] while the preparation and properties of RGO/Ni nanocomposites have rarely been studied. Recently, Gotoh *et al.* successfully deposited Ni nanoparticles onto RGO sheets from

[a]*School of Chemistry and Chemical Engineering, Jiangsu University, Zhenjiang, 212013, China. E-mail: xiaopingshen@163.com*
[b]*School of Materials Science and Engineering, Jiangsu University, Zhenjiang, 212013, China*
[c]*School of Materials Science and Engineering, Jiangsu University of Science and Technology, Zhenjiang, 212003, China*

† Electronic supplementary information (ESI) available: AFM image of RGO/Ni-1 nanocomposites, nitrogen adsorption and desorption isotherms of the RGO/Ni nanocomposites. See DOI: 10.1039/c2jm14680k

cation exchanged graphite oxide.[44] However, long experimental time and high-temperature calcination are required during the procedure, and the properties of the as-prepared RGO/Ni nanocomposites are not studied yet.

Herein, we present a facile low-temperature solution method for the large-scale synthesis of RGO/Ni nanocomposites. The morphology of the obtained RGO/Ni nanocomposites can be tuned by changing the starting amount of source materials and an interesting RGO-wrapped nanostructure was successfully prepared. The magnetic and catalytic properties of these nanocomposites are investigated. It was found that the catalytic activity of the RGO/Ni nanocomposites is even higher than RANEY® Ni for the reduction reaction of *p*-nitrophenol into *p*-aminophenol.

Experimental

Materials

Natural flake graphite was purchased from Qingdao Guyu Graphite Co., Ltd., with a particle size of 150 μm (99.9% purity). All of the other chemical reagents used in our experiments are of analytical grade, purchased from Sinopharm Chemical Reagent Co., Ltd., and used without further purification.

Preparation of graphite oxide

Graphite oxide was prepared from the natural flake graphite according to a modified Hummers method.[45] In a typical synthesis, 2.0 g of graphite powder was added to 80 mL of cold (0 °C) concentrated H_2SO_4 in an ice bath. Then, $NaNO_3$ (4.0 g) and $KMnO_4$ (8.0 g) were added gradually under stirring and the temperature of the mixture was kept to be below 10 °C. The reaction mixture was continually stirred for 4 h at temperature below 10 °C. Successively, the mixture was stirred at 35 °C for 4 h, and then diluted with 200 mL of deionized (DI) water. Because the addition of water in concentrated sulfuric acid medium releases a large amount of heat, the addition of water was performed in an ice bath to keep the temperature below 100 °C. After adding all of the 200 mL of DI water, the mixture was stirred for 1 h. The reaction was then terminated by adding 15 mL of 30% H_2O_2 solution. The solid product was separated by centrifugation, washed repeatedly with 5% HCl solution until sulfate could not be detected with $BaCl_2$. For further purification, the resulting solid was re-dispersed in DI water and then was dialyzed for three days to remove residual salts and acids. The suspension was dried in a vacuum oven at 45 °C for 48 h to obtain graphite oxide.

Preparation of RGO/Ni nanocomposites

In a typical synthesis of the RGO/Ni nanocomposites, 35 mg of graphite oxide was dispersed in 70 mL of DI water by ultrasonication to form a stable graphene oxide colloid, which was then mixed with 20 mL of $NiCl_2$ aqueous solution (containing 184 or 368 mg of $NiCl_2 \cdot 6H_2O$). Subsequently, 5 mL of hydrazine hydrate (85 wt%) were added into the mixed solution. The pH value of this mixture was adjusted to 10.5 by dropping 0.375 M NaOH aqueous solution. After ultrasonication for 10 min, the above mixture was transferred into a 250 mL round-bottomed flask and refluxed at 100 °C for 3 h under N_2 atmosphere. The as-synthesized solid products were separated by centrifugation, washed thoroughly with water and absolute ethanol to remove any impurities, and then dried in vacuum oven at 50 °C for 24 h. The products were signed as RGO/Ni-1 and RGO/Ni-2 for the feeding amount of 184 and 368 mg of $NiCl_2 \cdot 6H_2O$, respectively. In order to quantitatively analyze the weight content of Ni in RGO/Ni-1 and RGO/Ni-2, a certain amount of the nanocomposites was dispersed in diluted hydrochloric acid to dissolve Ni completely. After this treatment, the residue, which only contained RGO nanosheets, was washed by DI water, and dried in vacuum. By weighing the dried residue, the contents of Ni in RGO/Ni-1 and RGO/Ni-2 nanocomposites were determined to be *ca.* 65 and 80 wt%, respectively. As a comparison, pure Ni (named Ni-1 and Ni-2 corresponding to RGO/Ni-1 and RGO/Ni-2, respectively) and bare RGO were also synthesized in the same way as the nanocomposites in the absence of graphite oxide and $NiCl_2$, respectively. RANEY® Ni catalyst was prepared according to the literature method.[46]

Instrumentation and measurements

The morphology and structure of the products were determined by transmission electron microscopy (TEM, JEOL JEM-2100) and X-ray diffraction (XRD, Bruker D8 ADVANCE) with Cu-Kα radiation. Samples for TEM observation were prepared by dropping the products on a carbon-coated copper grid after ultrasonic dispersion in absolute ethanol. Raman scattering was performed on a JY-HR800 Raman spectrometer using a 453 nm laser source. Atomic force microscopy (AFM) measurement was conducted using a multi-mode scanning probe microscope. Samples for AFM imaging were prepared by spin-coating of the nanocomposite suspension onto freshly cleaved mica substrate, which were then allowed to dry in air. The Brunauer-Emmett-Teller (BET) surface area of the products were tested using an ASAP 2010 sorption analyzer. The magnetic properties of the products were measured by vibrating sample magnetometer (VSM, Nanjing University HH-15) at room temperature (300 K). Ultraviolet-visible (UV-vis) spectroscopy measurements were performed on a UV-2450 ultraviolet-visible spectrophotometer.

Catalytic study

The reduction reaction of *p*-nitrophenol by $NaBH_4$ was used as a model system to quantitatively evaluate the catalytic activity of the as-synthesized nanocomposites. In a typical procedure, the aqueous solutions of *p*-nitrophenol (5 mM) and $NaBH_4$ (1.5 M) were freshly prepared. 2 mL of $NaBH_4$ solution and a certain amount of catalysts containing 6.5 mg of nickel were added to 100 mL of DI water. Then, 2 mL of *p*-nitrophenol solution was injected into the mixture to start the reaction. During the reaction process, 1 mL of the reaction solution was withdrawn from the reaction system at a regular time interval of 20 min, and diluted with 2 mL of DI water followed by measuring UV-vis spectra of the solution to monitor the concentration of *p*-nitrophenol through its absorption peak at 400 nm.

Results and discussion

Structural and morphological characterization

The phase structure of the as-synthesized samples was firstly determined by X-ray diffraction (XRD). As shown in Fig. 1, the original graphite oxide sample shows a sharp peak at $2\theta = 10.3°$, corresponding to the (001) reflection of graphite oxide.[47] However, the characteristic peak of graphite oxide can not be observed in the XRD patterns of RGO/Ni-1 and RGO/Ni-2 nanocomposites, suggesting graphite oxide was effectively reduced. The characteristic (111), (200), (220) peaks which can be easily indexed to cubic Ni (JCPDS 04-0850) are all observed in RGO/Ni-1 and RGO/Ni-2 samples, indicating that nickel ions have been reduced into metal Ni after the reducing process and no detectable impurities such as $Ni(OH)_2$ exist in the samples.

Raman spectroscopy is a suitable technique to characterize carbonaceous materials, particularly for distinguishing ordered and disordered crystal structures of carbon. The typical Raman spectra of graphite oxide, RGO/Ni-1 and RGO/Ni-2 nanocomposites are shown in Fig. 2. They all display two prominent peaks, which correspond to the well-documented G and D bands. The G band is usually assigned to the E_{2g} phonon of C sp^2 atoms, while the D band originates from a breathing κ-point phonon with A_{1g} symmetry and related to local defects and disorders.[48,49] The G band moved from 1603 cm^{-1} of graphite oxide to *ca.* 1586 cm^{-1} of RGO/Ni nanocomposites, close to the value of the pristine graphite, confirming the reduction of graphite oxide.[50] The intensity ratio (I_D/I_G) of the D band to the G band is correlative with the average size of sp^2 domains,[13] that is, the smaller size of sp^2 domains, the higher intensity ratio (I_D/I_G). The I_D/I_G ratios for graphite oxide, RGO/Ni-1 and RGO/Ni-2 are 1.11, 1.43 and 1.50, respectively. The increase of I_D/I_G ratios for RGO/Ni nanocomposites as compared with graphite oxide is reasonable because after chemical reduction of graphene oxide, the conjugated graphene network (sp^2 carbon) will be re-established, however, the size of the re-established graphene network is usually smaller than the original graphite layer, which will lead to the increase of intensity ratio (I_D/I_G) consequently.[51] Thus, it is concluded that graphite oxide in RGO/Ni nanocomposites has been well deoxygenated and reduced.

The morphology of the as-prepared RGO/Ni nanocomposites was examined by transmission electron microscopy (TEM) and high resolution transmission electron microscopy (HRTEM). Fig. 3 shows the TEM images of RGO/Ni-1 nanocomposites. Crumpled silk waves-like morphology, a characteristic feature of the single-layer graphene sheets, is observed in Fig. 3a. Ni nanoparticles can hardly be observed from this TEM image owing to their small size. The cross section analysis of AFM (Fig. S1, ESI†) indicates a height of 0.993 nm for the RGO sheet in RGO/Ni-1 nanocomposites, which is in good consistency with the reported apparent thickness of single layer RGO sheet.[15] Fig. 3b and c present the higher magnification TEM images of RGO/Ni-1 nanocomposites. It can be seen that Ni nanoparticles are densely and uniformly distributed on the surfaces of graphene sheets. Almost no free Ni nanoparticles are found outside of the RGO sheets throughout the TEM observation process, indicating the perfect combination between Ni nanoparticles and RGO nanosheets. The HRTEM image shown in Fig. 3d clearly demonstrates the homogeneous distribution of the Ni nanoparticles with uniform size of 2–4 nm on RGO sheets. The lattice fringes with a spacing of 0.202 nm are clearly observed in the inset of Fig. 3d, which can be indexed as the (111) crystal plane of cubic Ni.

The concentration of the source materials has a great influence on the morphology of the as-prepared RGO/Ni nanocomposites. When the starting amount of $NiCl_2 \cdot 6H_2O$ used was increased to

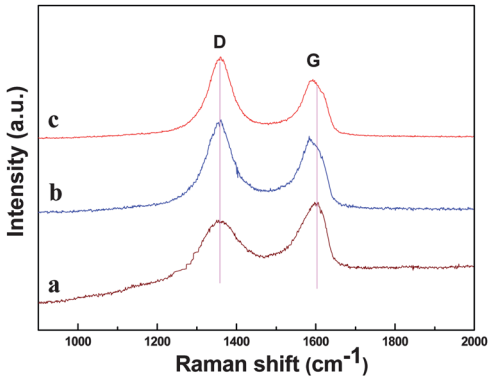

Fig. 2 Raman spectra of (a) graphite oxide, (b) RGO/Ni-1 and (c) RGO/Ni-2 nanocomposites.

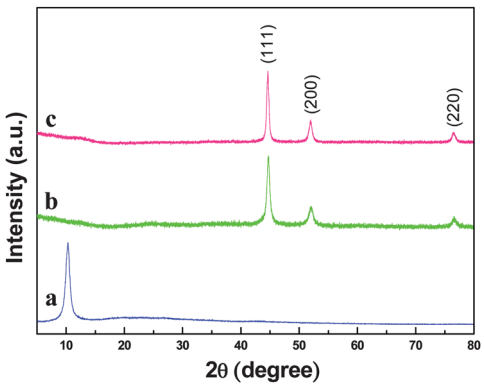

Fig. 1 XRD patterns of (a) graphite oxide, (b) RGO/Ni-1 and (c) RGO/Ni-2 nanocomposites.

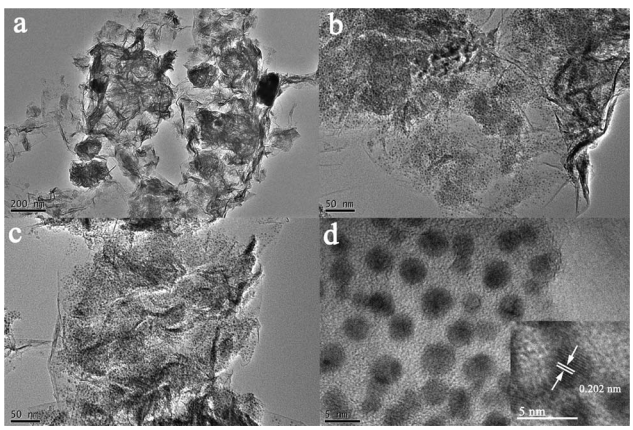

Fig. 3 (a)–(c) TEM and (d) HRTEM images of the RGO/Ni-1 nanocomposites.

276 mg, the mean diameter of Ni nanoparticles was increased to about 40 nm and the as-formed Ni nanoparticles were also well deposited on the surface of the RGO sheets (Fig. 4). The increase of the size of Ni nanoparticles is understandable. Graphene oxide is negatively charged due to the abundant hydroxyl and carboxyl groups. When the nickel salts were introduced into the graphene oxide suspension, nickel ions would attach to the surface of graphene oxide through electrostatic interaction and serve as nucleation sites. When the reductant N_2H_4 was introduced, the nickel ions were *in situ* reduced to form nuclei, while graphene oxide nanosheets were reduced to RGO at the same time. With higher concentration of nickel chloride, more metal ions were reduced and absorbed on the nuclei, and then they grew into larger spherical nanoparticles. Further increasing the amount of nickel chloride not only induces the increase of Ni nanoparticle size, but also can cause the change of composite structure. For example, as can be seen from the TEM images of RGO/Ni-2 nanocomposites (Fig. 5), when 368 mg of $NiCl_2 \cdot 6H_2O$ was used, the size of the obtained Ni nanoparticles was increased to about 80–160 nm. Moreover, the Ni nanoparticles were almost fully wrapped by RGO sheets rather than simply deposited on the surface, resulting in an interesting RGO-wrapped composite structure. Such a composite structure is different from conventional RGO-based nanocomposites and has not been reported before. In this structure, RGO sheets can act as a protection layer to prevent the encapsulated metals from environmental oxidation, and avoid the exfoliation of the loading components from the RGO sheets. The formation process of the RGO-wrapped-Ni nanocomposites (RGO/Ni-2 nanocomposites) can be proposed as follows: the original graphene oxide or RGO sheets in the reaction system are uniformly suspended in the solvent owing to the rich hydrophilic groups. When Ni nanoparticles are deposited on them, the gravity of them would cause them to subside. The subsiding trend becomes stronger with the bigger Ni nanoparticles. Thus, it is probable when the bigger Ni nanoparticles with size of 80–160 nm are deposited on the RGO sheets, the gravity of them will cause them to subside together. In the subsiding process, Ni nanoparticles push down the flexible RGO sheets and make them curl down to form a coated composite structure. On the other hand, the RGO sheets tend to aggregate in solution during the reduction process, which is also helpful to form the wrapped morphology of the RGO/Ni-2 nanocomposites.

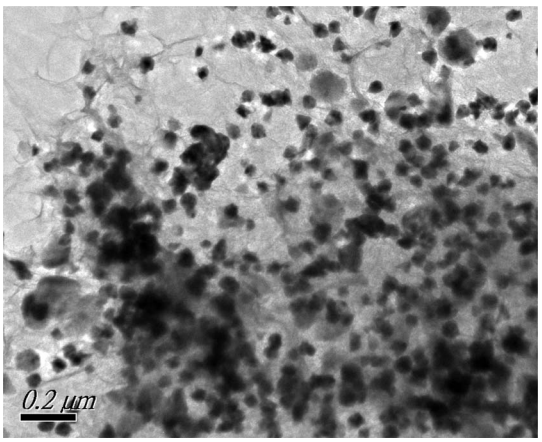

Fig. 4 TEM image of the RGO/Ni nanocomposites prepared with 276 mg of $NiCl_2 \cdot 6H_2O$.

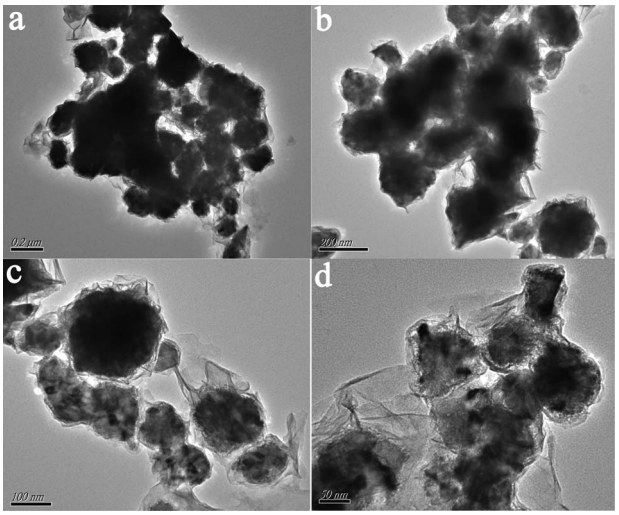

Fig. 5 TEM images of the RGO/Ni-2 nanocomposites.

The specific surface areas of the RGO/Ni nanocomposites were investigated by BET technique. Based on the adsorption branch of isotherm curves (Fig. S2, ESI†), the specific surface areas are calculated to be 192.39 and 81.37 $m^2\ g^{-1}$ for RGO/Ni-1 and RGO/Ni-2, respectively. It is well known that the theoretical specific surface area of graphene is as high as 2630 $m^2\ g^{-1}$.[1] However, the specific surface area of the graphene-based nanocomposite materials is much lower than the theoretical value due to the bigger weight contribution from nanoparticles on the surface of graphene sheets.[52] Moreover, the specific surface area of graphene-based nanocomposites decreases with increasing amount of the loaded nanoparticles.[38,53] This phenomena has also been observed by other researchers in many cases. For example, although the agglomeration of RGO sheets was hindered by Cu_2O nanoparticles, the Cu_2O/RGO composite exhibited a low specific surface area of 92.2 $m^2\ g^{-1}$.[52] The specific surface area of graphene-based nanocomposites was even decreased to 2.3 $m^2\ g^{-1}$ when the content of graphene was 5 wt% in the case of CdS/RGO composite.[54] Therefore, it is reasonable that our prepared RGO/Ni-1 and RGO/Ni-2 nanocomposites with high Ni-loading (65 and 80 wt%) show low specific surface area as compared with pure graphene. The larger specific surface area of RGO/Ni-1 than RGO/Ni-2 could be attributed to the lower content and smaller size of the Ni nanoparticles in RGO/Ni-1 nanocomposites.

Magnetic properties

The magnetic properties of the as-synthesized RGO/Ni-1 and RGO/Ni-2 nanocomposites were investigated at room temperature. Both RGO/Ni-1 and RGO/Ni-2 nanocomposites exhibit typical ferromagnetic behavior (Fig. 6) with a saturation magnetization of 19.1 and 35.7 emu g^{-1}, respectively. The saturation magnetization (M_s) values of Ni in the composites were calculated to be 29.4 and 44.6 emu g^{-1} Ni, which are smaller than the reported value of bulk Ni (55 emu g^{-1}).[55] This can be

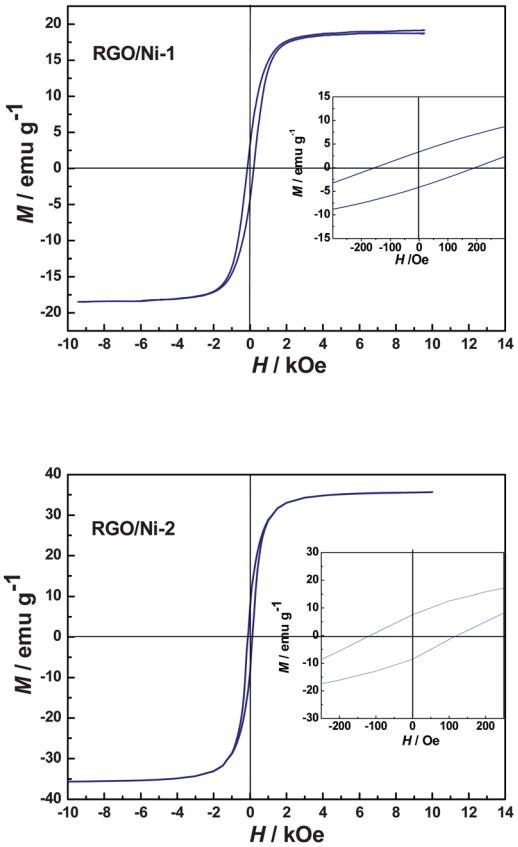

Fig. 6 Magnetic hysteresis loops of RGO/Ni-1 and RGO/Ni-2 nanocomposites at 300 K. The inset is magnified hysteresis loop in low field zone.

attributed to the small particle size of Ni nanoparticles in the composites, which can decrease the effective magnetic moment of Ni.[56] The coercivity (H_c) is determined to be 179 Oe for RGO/Ni-1 and 118 Oe for RGO/Ni-2 nanocomposites. The H_c of RGO/Ni-1 is larger than that of RGO/Ni-2 and bulk Ni (100 Oe). This may originate from the smaller size, which may change the magnetization reversal mechanism and lead to a higher coercivity.[57] The other parameters such as internal stress, orientation, defects, and morphology would also contribute to the increase of coercivity since it is sensitive to many structural parameters.[58]

It is worth noting that Ni nanoparticles with a size of *ca.* 2–4 nm are single magnetic domain owing to the small size, and usually display superparamagnetic behavior under ambient conditions.[56,59] It seems that the ferromagnetic-like behavior of the RGO/Ni-1 sample inherently correlates with the existence of interaction between RGO and Ni, through which electronic structure modifications and symmetry breaking could influence the magnetic anisotropy term. The RGO/Ni-1 nanocomposites would have potential applications in data storage, since this room-temperature ferromagnetic-like behavior with particle size of Ni below single domain size is highly expected in this field.[39] In addition, the RGO/Ni-2 nanocomposites with RGO-wrapped structure may find applications in targeted drug transportation and magnetic resonance imaging technology in respect that graphene is highly biocompatible and stable in ambient conditions. Particularly, the carbon-wrapped magnetic nanoparticles could also be used as catalyst carriers for loading catalytically active species on their surfaces, which might facilitate the separation of expensive catalyst species from products by an external magnetic field.[27]

Catalytic properties

The reduction of aromatic nitro compounds to amines is a very important process in synthetic organic chemistry and in industrial fabrication of many industrially important products. In this study, the reduction of *p*-nitrophenol into *p*-aminophonol by $NaBH_4$ was employed as a model reaction to quantitatively evaluate the catalytic activity of the as-synthesized nanocomposites. This reaction has been demonstrated to be useful for the analysis of the catalytic activity of noble metal.[60–62] Controlled experiments have shown that the reduction reaction does not take place in the absence of catalysts or presence of pure RGO, even with a period of two days. It is well known that *p*-nitrophenol exhibits a strong absorption peak at 400 nm in alkaline solution.[63,64] As the reduction reaction proceeded, the intensity of the absorption peak at 400 nm gradually decreased. Fig. 7 shows the UV-vis spectra of the diluted reaction solution measured at every 20 min intervals using RGO/Ni-1 nanocomposites as catalyst. It can be seen that the absorption associated with *p*-nitrophenol at 400 nm decreases with a concomitant increase of the absorption at 300 nm from *p*-aminophenol as the reduction reaction proceeded. These results indicate that RGO/Ni-1 nanocomposites can successfully catalyze the reduction reaction due to the presence of Ni.

In the reduction process, as excess $NaBH_4$ was used, the BH_4^- concentration can be considered as a constant throughout the reaction. The UV-vis spectra also exhibit an isosbestic point between two absorption bands, indicating that only two principal species, *p*-nitrophenol and *p*-aminophenol, influence the reaction kinetics.[65] Therefore, pseudo first order kinetics could be applied for the evaluation of rate constants in this case. The ratio of absorbance A (at peak of 400 nm) of *p*-nitrophenol at time t to its original value A_0 measured at $t = 0$ directly gives the corresponding concentration ratio C/C_0 of *p*-nitrophenol. Thus the kinetic equation of the reduction reaction could be given as follows:

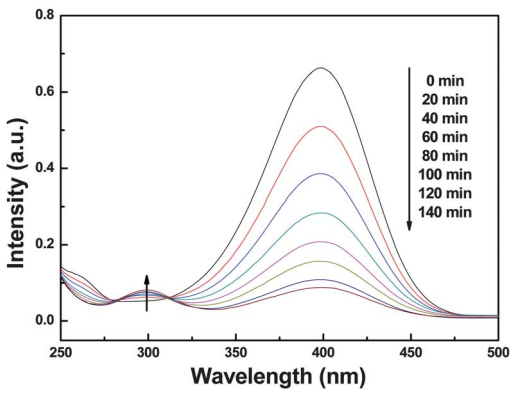

Fig. 7 Successive UV-vis spectra for the reduction reaction of *p*-nitrophenol by $NaBH_4$ with RGO/Ni-1 as a catalyst.

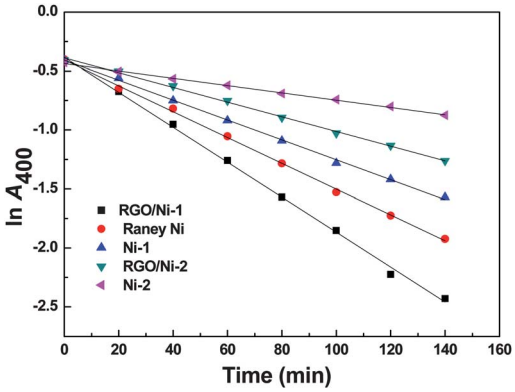

Fig. 8 Pseudo first order plot of $\ln A_{400}$ *versus* reaction time for the reduction of *p*-nitrophenol catalyzed by different catalysts.

$$kt = \ln C_0 - \ln C = \ln A_0 - \ln A$$

where C and C_0 are the concentration of *p*-nitrophenol at time t and $t = 0$, respectively; k is the apparent rate constant. The kinetic parameters of the reduction reaction can be obtained by monitoring the absorbance at 400 nm (A_{400}) as a function of time. The relations of $\ln A_{400}$ *versus* t under different catalysts are shown in Fig. 8. It is clear that $\ln A_{400}$ shows good linear correlation with the reaction time for all catalysts, indicating that the reaction follows first-order kinetics. The rate constants for different catalysts were estimated from diffusion-coupled first order reaction kinetics using the slopes of the straight lines and are given in Table 1. The rate constant for RGO/Ni-1 (or RGO/Ni-2) nanocomposites is almost two times higher than that obtained for Ni-1 (or Ni-2) with free Ni nanoparticles, indicating that the catalytic activity of Ni nanoparticles can be remarkably improved by combining them with RGO sheets. Such an enhancement in catalytic activity can be attributed to the following two factors: (i) Due to the peculiar electronic structure of RGO, the nanocomposites may possess high migration efficiency of electrons, which play an important role in enhancing the catalytic activity for the reduction of *p*-nitrophenol.[64] (ii) As compared with bare Ni nanoparticles, RGO nanocomposites can offer an environment to prevent aggregation of Ni nanoparticles and obstruct facile loss of activity. It should be noted that the RGO/Ni-1 exhibits a higher catalytic activity than RGO/Ni-2. This may be due to the smaller size of Ni nanoparticles and higher surface area of RGO/Ni-1 as compared with those of RGO/Ni-2 nanocomposites.

For further estimation of these composite catalysts, RANEY® Ni catalyst was also prepared and tested for this reduction reaction under the same reaction conditions. It was found that the catalytic activity of RGO/Ni-1 was even higher than that of RANEY® Ni catalyst, indicating the excellent catalytic performance of the RGO/Ni nanocomposites. Moreover, the ferromagnetic property of the RGO/Ni nanocomposites is useful for separating the catalysts from the reaction system by a magnet. This economical and easy method for the synthesis of RGO-nickel catalyst together with its high catalytic activity provides a potentially new approach for the design and construction of the nanostructured catalysts with excellent performance.

Conclusions

In summary, RGO/Ni nanocomposites with different morphologies were successfully synthesized by a facile *in situ* reduction approach. The starting amount of the nickel chloride has a great influence on the size of Ni nanoparticles and the composite morphology. The size of the Ni nanoparticles on RGO sheets can be tuned from below 5 nm to several tens of nanometres. Magnetic studies reveal that the RGO/Ni nanocomposites display room-temperature ferromagnetic behavior, even for the nanocomposites with 2–4 nm Ni nanoparticles. This unique magnetic properties make them promising for practical applications in future nanodevices. In addition, the composites show remarkably improved catalytic activity in the reduction of *p*-nitrophenol. The catalytic performance of RGO/Ni nanocomposites was even higher than the industrial RANEY® Ni catalyst. Thus, the RGO/Ni nanocomposites with good magnetic and catalytic properties may find applications in many fields such as catalysis, data storage and biomedicine. The enhanced catalytic performances arising from synergistic coupling between nanoparticles and RGO may open up a new approach to advanced catalysts.

Acknowledgements

The authors are grateful for financial support from the Natural Science Foundation of Jiangsu Province (No. BK2009196) and the National Natural Science Foundation of China (No. 51072071).

Notes and references

1 S. Park and R. S. Ruoff, *Nat. Nanotechnol.*, 2009, **4**, 217.
2 A. K. Geim and K. S. Novoselov, *Nat. Mater.*, 2007, **6**, 183.
3 M. J. Allen, V. C. Tung and R. B. Kaner, *Chem. Rev.*, 2009, **110**, 132.
4 C. N. R. Rao, A. K. Sood, K. S. Subrahmanyam and A. Govindaraj, *Angew. Chem., Int. Ed.*, 2009, **48**, 7752.
5 S. Stankovich, D. A. Dikin, G. H. B. Dommett, K. M. Kohlhaas, E. J. Zimney, E. A. Stach, R. D. Piner, S. T. Nguyen and R. S. Ruoff, *Nature*, 2006, **442**, 282.
6 S. Watcharotone, D. A. Dikin, S. Stankovich, R. Piner, I. Jung, G. H. B. Dommett, G. Evmenenko, S. E. Wu, S. F. Chen, C. P. Liu, S. T. Nguyen and R. S. Ruoff, *Nano Lett.*, 2007, **7**, 1888.
7 G. Williams, B. Seger and P. V. Kamat, *ACS Nano*, 2008, **2**, 1487.
8 S. M. Paek, E. Yoo and I. Honma, *Nano Lett.*, 2009, **9**, 72.
9 K. S. Novoselov, A. K. Geim, S. V. Morozov, D. Jiang, Y. Zhang, S. V. Dubonos, I. V. Grigorieva and A. A. Firsov, *Science*, 2004, **306**, 666.

Table 1 The rate constants for the reduction reaction of *p*-nitrophenol under different catalysts and the correlation coefficient for $\ln A$–t plots

Samples	RGO/Ni-1	RGO/Ni-2	Ni-1	Ni-2	RANEY® Ni
k ($\times 10^{-3}$ min^{-1})	14.82	6.23	8.45	3.10	10.95
R^2	0.9979	0.9981	0.9985	0.9978	0.9986

10 K. S. Kim, Y. Zhao, H. Jang, S. Y. Lee, J. M. Kim, K. S. Kim, J. H. Ahn, P. Kim, J. Y. Choi and B. H. Hong, *Nature*, 2009, **457**, 706.
11 H. C. Schniepp, J. L. Li, M. J. McAllister, H. Sai, M. Herrera-Alonso, D. H. Adamson, R. K. Prud'homme, R. Car, D. A. Saville and I. A. Aksay, *J. Phys. Chem. B*, 2006, **110**, 8535.
12 A. Reina, X. T. Jia, J. Ho, D. Nezich, H. B. Son, V. Bulovic, M. S. Dresselhaus and J. Kong, *Nano Lett.*, 2009, **9**, 30.
13 S. Stankovich, D. A. Dikin, R. D. Piner, K. A. Kohlhaas, A. Kleinhammes, Y. Jia, Y. Wu, S. T. Nguyen and R. S. Ruoff, *Carbon*, 2007, **45**, 1558.
14 X. B. Fan, W. C. Peng, Y. Li, X. Y. Li, S. L. Wang, G. L. Zhang and F. B. Zhang, *Adv. Mater.*, 2008, **20**, 4490.
15 D. Li, M. B. Muller, S. Gilje, R. B. Kaner and G. G. Wallace, *Nat. Nanotechnol.*, 2008, **3**, 101.
16 H. J. Shin, K. K. Kim, A. Benayad, S. M. Yoon, H. K. Park, I. S. Jung, M. H. Jin, H. K. Jeong, J. M. Kim, J. Y. Choi and Y. H. Lee, *Adv. Funct. Mater.*, 2009, **19**, 1987.
17 A. Buchsteiner, A. Lerf and J. Pieper, *J. Phys. Chem. B*, 2006, **110**, 22328.
18 K. Jasuja and V. Berry, *ACS Nano*, 2009, **3**, 2358.
19 B. J. Li, H. Q. Cao, J. Shao, H. Zheng, Y. X. Lu, J. F. Yin and M. Z. Qu, *Chem. Commun.*, 2011, **47**, 3159.
20 Q. Li, B. D. Guo, J. G. Yu, J. R. Ran, B. H. Zhang, H. J. Yan and J. R. Gong, *J. Am. Chem. Soc.*, 2011, **133**, 10878.
21 G. M. Scheuermann, L. Rumi, P. Steurer, W. Bannwarth and R. Mulhaupt, *J. Am. Chem. Soc.*, 2009, **131**, 8262.
22 Y. Y. Liang, Y. G. Li, H. L. Wang, J. G. Zhou, J. Wang, T. Regier and H. J. Dai, *Nat. Mater.*, 2011, **10**, 780.
23 S. Chikazumi, S. Taketomi, M. Ukita, M. Mizukami, H. Miyajima, M. Setogawa and Y. Kurihara, *J. Magn. Magn. Mater.*, 1987, **65**, 245.
24 D. Chiba, M. Sawicki, Y. Nishitani, Y. Nakatani, F. Matsukura and H. Ohno, *Nature*, 2008, **455**, 515.
25 A. K. Gupta and M. Gupta, *Biomaterials*, 2005, **26**, 3995.
26 A. H. Lu, W. Schmidt, N. Matoussevitch, H. Bpnnermann, B. Spliethoff, B. Tesche, E. Bill, W. Kiefer and F. Schuth, *Angew. Chem., Int. Ed.*, 2004, **43**, 4303.
27 S. C. Tsang, V. Caps, I. Paraskevas, D. Chadwick and D. Thompsett, *Angew. Chem., Int. Ed.*, 2004, **43**, 5645.
28 S. Mornet, S. Vasseur, F. Grasset, P. Verveka, P. Goglio, A. Demourgues, J. Portier, E. Pollert and E. Duguet, *Prog. Solid State Chem.*, 2006, **34**, 237.
29 Z. Li, L. Wei, M. Y. Gao and H. Lei, *Adv. Mater.*, 2005, **17**, 1001.
30 Y. S. Fu and X. Wang, *Ind. Eng. Chem. Res.*, 2011, **50**, 7210.
31 X. Y. Yang, X. Y. Zhang, Y. F. Ma, Y. Huang, Y. S. Wang and Y. S. Chen, *J. Mater. Chem.*, 2009, **19**, 2710.
32 H. M. Sun, L. Y. Cao and L. H. Lu, *Nano Res.*, 2011, **4**, 550.
33 M. Zhang, D. N. Lei, X. M. Yin, L. B. Chen, Q. H. Li, Y. G. Wang and T. H. Wang, *J. Mater. Chem.*, 2010, **20**, 5538.
34 B. J. Li, H. Q. Cao, J. Shao, M. Z. Qu and J. H. Warner, *J. Mater. Chem.*, 2011, **21**, 5069.
35 B. J. Li, H. Q. Cao, J. Shao and M. Z. Qu, *Chem. Commun.*, 2011, **47**, 10374.
36 H. P. Cong, J. J. He, Y. Lu and S. H. Yu, *Small*, 2010, **6**, 169.
37 G. X. Zhu, Y. J. Liu, Z. Xu, T. Jiang, C. Zhang, X. Li and G. Qi, *ChemPhysChem*, 2010, **11**, 2432.
38 N. W. Li, M. B. Zheng, X. F. Chang, G. B. Ji, H. L. Lu, L. P. Xue, L. J. Pan and J. M. Cao, *J. Solid State Chem.*, 2011, **184**, 953.
39 Z. Y. Ji, X. P. Shen, Y. Song and G. X. Zhu, *Mater. Sci. Eng., B*, 2011, **176**, 711.
40 R. Xu, T. Xie, Y. G. Zhao and Y. D. Li, *Nanotechnology*, 2007, **18**, 055602.
41 C. L. Tang, L. P. Li, H. B. Gao, G. S. Li, X. Q. Qiu and J. Liu, *J. Power Sources*, 2009, **188**, 397.
42 A. Gotoh, H. Uchida, M. Ishizaki, T. Satoh, S. Kaga and S. Okamoto, *Nanotechnology*, 2007, **18**, 345609.
43 A. E. Virden and K. O'Grady, *J. Appl. Phys.*, 2006, **99**, 08S106.
44 K. Gotoh, T. Kinumoto, E. Fujii, A. Yamamoto, H. Hashimoto, T. Ohkubo, A. Itadani, Y. Kuroda and H. Ishida, *Carbon*, 2010, **49**, 1118.
45 W. S. Hummers and R. E. Offeman, *J. Am. Chem. Soc.*, 1958, **80**, 1339.
46 A. L. Wang, H. B. Yin, H. H. Lu, J. J. Xue, M. Ren and T. S. Jiang, *Langmuir*, 2009, **25**, 12736.
47 T. Nakajima, A. Mabuchi and R. Hagiwara, *Carbon*, 1988, **26**, 357.
48 F. Tuinstra and J. L. Koenig, *J. Chem. Phys.*, 1970, **53**, 1126.
49 D. Graf, F. Molitor, K. Ensslin, C. Stampfer, A. Jungen, C. Hierold and L. Wirtz, *Nano Lett.*, 2007, **7**, 238.
50 W. F. Chen, L. F. Yan and P. R. Bangal, *J. Phys. Chem. C*, 2010, **114**, 19885.
51 C. Xu, X. Wang and J. W. Zhu, *J. Phys. Chem. C*, 2008, **112**, 19841.
52 B. J. Li, H. Q. Cao, G. Yin, Y. X. Lu and J. F. Yin, *J. Mater. Chem.*, 2011, **21**, 10645.
53 V. Chandra, J. Park, Y. Chun, J. W. Lee, I. C. Hwang and K. S. Kim, *ACS Nano*, 2010, **4**, 3979.
54 L. Jia, D. H. Wang, Y. X. Huang, A. W. Xu and H. Q. Yu, *J. Phys. Chem. C*, 2011, **115**, 11466.
55 X. C. Sun and X. L. Dong, *Mater. Res. Bull.*, 2002, **37**, 991.
56 S. H. Wu and D. H. Chen, *J. Colloid Interface Sci.*, 2003, **259**, 282.
57 X. W. Wei, G. X. Zhu, Y. J. Liu, Y. H. Ni, Y. Song and Z. Xu, *Chem. Mater.*, 2008, **20**, 6248.
58 T. Hayashi, S. Hirono, M. Tomita and S. Umemura, *Nature*, 1996, **381**, 772.
59 Y. L. Hou and S. Gao, *J. Mater. Chem.*, 2003, **13**, 1510.
60 T. Y. Yu, J. Zeng, B. Lim and Y. N. Xia, *Adv. Mater.*, 2010, **22**, 5188.
61 M. Schrinner, M. Ballauff, Y. Talmon, Y. Kauffmann, J. Thun, M. Moller and J. Breu, *Science*, 2009, **323**, 617.
62 Y. Mei, Y. Lu, F. Polzer, M. Ballauff and M. Drechsler, *Chem. Mater.*, 2007, **19**, 1062.
63 S. Praharaj, S. Nath, S. K. Ghosh, S. Kundu and T. Pal, *Langmuir*, 2004, **20**, 9889.
64 J. Zeng, Q. Zhang, J. Y. Chen and Y. N. Xia, *Nano Lett.*, 2010, **10**, 30.
65 J. Lee, J. C. Park and H. Song, *Adv. Mater.*, 2008, **20**, 1523.